Residual Stresses in Weld Thermal Cycle Simulated Specimens of X70 Pipeline Steel

The forces caused by the constrained expansion and contraction of X70 pipeline steel specimens, subjected to simulated weld thermal cycles, were measured by means of Satoh testing

BY M. I. ONSØIEN, M. M'HAMDI, AND O. M. AKSELSEN

ABSTRACT

The present work concerns Satoh testing of X70 pipeline steel and was undertaken in order to assess residual stresses in steel weldments. Experiments using single, double, and triple temperature cycles were performed to study how different temperature histories affected the development of residual stresses in the tested specimens. In some of the single-cycle experiments, high tensile stresses or high compressive stresses were imposed on the sample at the start of the experiment to study the response of the sample to preloading. Residual stresses higher than 490 MPa have been measured. It was further found that samples with low austenite transformation temperature may build up higher residual stress than samples with higher austenite transformation temperature. A prerequisite for this behavior is that the transformation product in the first case has high yield strength and the transformation product in the second case reaches its yield limit. It is also shown that the effect of preloading on the shape of the σ-T curve is negligible for temperatures above the A_{c1} temperature, i.e., the phase transformation relaxes the effect of different initial stresses and the final stress level is very similar for samples starting in high compression, high tension, or zero stress. It is further shown that the effect of multiple cycles on the shape of the σ-T curve and on the final stress level is low, probably because of stress-strain relaxation during the phase transformations.

Introduction

The heat generated during welding causes a high temperature gradient in and around the welded area. This leads to nonuniform expansion and contraction of the material causing buildup of stresses. The stresses that are not recovered by elasticity in the material become residual stresses that might result in severe distortion and premature failure. Thermophysical properties such as heat capacity, thermal expansion coefficient, and density, as well as mechanical properties such as the elastic modulus and yield strength, contribute to the type and magnitude of residual stresses (Refs. 1–3).

Residual stresses may be determined by experimental means or estimated using numerical methods. Experimental methods include hole drilling (Ref. 4) and ultrasonic methods (Ref. 5) as well as X-ray and neutron diffraction methods (Refs. 6–9). Numerical methods, developed by a number of authors (Refs. 10, 11) using, e.g., a finite element code, allow the computation of residual stresses and their distributions based on input such as mechanical properties of the processed material, shape, and dimensions of the part, and loading conditions. However, the complexity of these methods limits their practical application. Often important material data are not available, and thorough descriptions of how the material data changes during a weld thermal cycle and during phase transformations are usually missing.

The aim of the present work is to analyze the stress development in the heat-affected zone (HAZ) of an X70 pipeline steel using the Satoh test (Refs. 12, 13). In this test, a specimen is mounted in a rigid steel frame and heated according to a controlled thermal cycle, simulating the heat cycle in the HAZ of a real weld. The forces created by the expansion and contraction of the specimen are recorded by means of a load cell and a data-acquisition system. The collected experimental data can be used for the verification or calibration of numerical simulations of residual stresses in steel weldments (Ref. 14).

M. I. ONSØIEN (morten.i.onsoien@sintef.no), *M. M'HAMDI, and O. M. AKSELSEN are with SINTEF Materials and Chemistry, Trondheim, Norway.*

KEYWORDS

Satoh Test
Residual Stress
Multipass Weld Simulation
Weld Thermal Cycle Simulation
API X70 Steel
Pipeline Steel

Materials and Experimental Procedure

The specimens for Satoh testing were machined from X70 pipeline steel with chemical composition and mechanical properties as given in Table 1. Metallographic analyses (Ref. 16) have shown that the material is composed of ferrite (86%) with bands of pearlite (14%). The average hardness is 200 HV_{10}. The continuous-cooling-temperature (CCT) diagram for the studied steel is given in Fig. 1.

The specimen geometry for Satoh testing is shown in Fig. 2. The Satoh test jig (Fig. 3) consists of a rigid welded steel frame into which the sample is mounted. An induction coil and a cooling gas (Ar or He) diffuser are mounted coaxially around the sample. This setup permits controlled heating and cooling of the sample according to the desired temperature cycle. The sample surface temperature is recorded by means of three chromel/alumel thermocouples (Type K) spot welded to the specimen gauge length, one at mid-length and one 10 mm above and one 10 mm below this position. During testing, expansion in the upper end is restrained by the top beam of the Satoh frame. Thus, the load cell in the lower end of the frame records the expansion of the specimen. The specimen fixtures are water-cooled to prevent thermal expansion of the jig, only expansion of the specimen is therefore imposed on the load cell (Ref. 15). Load cell and thermocouple signals are recorded by a

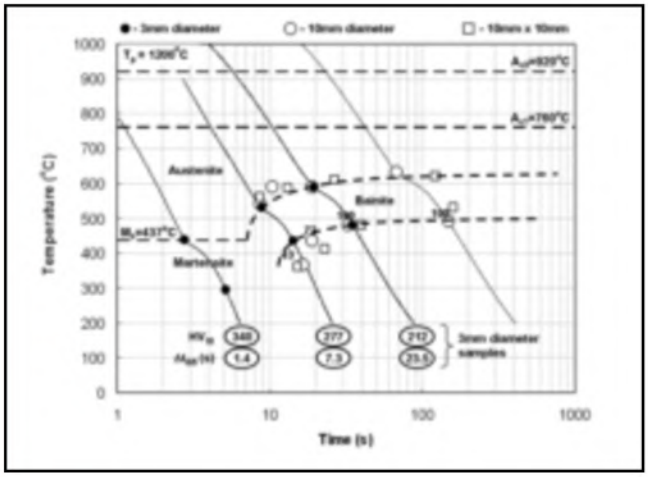

Fig. 1 — CCT diagram for X70 pipeline steel used in current experiments (Ref. 16).

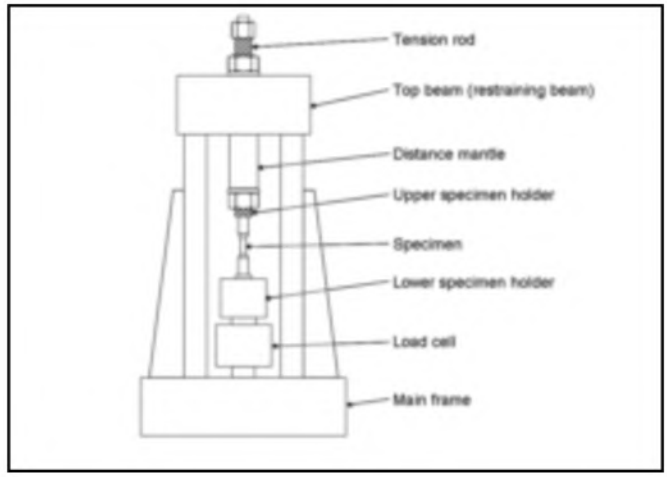

Fig. 3 — Schematic drawing of the Satoh test jig.

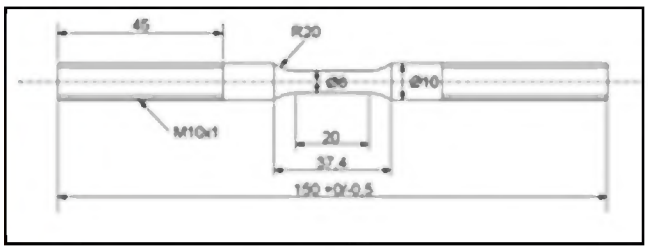

Fig. 2 — Specimen geometry for Satoh testing.

computer-controlled data-acquisition system. The heating cycles characterized by the peak temperature (T_p) and the cooling time from 800° to 500°C ($\Delta t_{8/5}$) are intended to resemble HAZ temperature cycles during real welding situations.

Experimental Program

Experiments using single, double, and triple temperature cycles were performed to study how different temperature histories affected the development of residual stresses in the tested specimens. Single-cycle experiments included heating to peak temperatures of about 1100°, 1200°, and 1350°C, prior to cooling using cooling time $\Delta t_{8/5}$ of about 10, 15, and 20 s. In some of the single-cycle experiments, a high tensile stress or a high compressive stress was imposed on the sample at the start of the experiment to study the response of the sample to preloading. Double-cycle experiments included heating to the first peak temperature, cooling down to 150°C, before heating to the second peak temperature and subsequent cooling to ambient temperature. Triple-cycle experiments included heating to the first peak temperature followed by cooling down to 150°C, prior to heating to the second peak temperature and cooling down to 150°C before heating to the third peak temperature followed by cooling to ambient temperature. The intermediate cooling temperature of 150°C is meant to represent the typical interpass temperature in a real welding situation. The main outline of the experimental program is given in Table 2.

Results and Discussion

Single Cycle Experiments

Figures 4 and 5 show temperature measurements in the center surface of the samples for various heating and cooling conditions. The heating rate in the ferrite region is around 680°C/s, while it is much lower, about 75°C/s, in the austenite region. Examples of recorded stress vs. center surface temperature (σ-T) curves for single-cycle experiments are shown in Figs. 6 and 7. During heating the samples expand and a compressive stress builds up due to the constrained axial displacement imposed by the rigid Satoh test frame. The compressive stress reaches its maximum, typically about 350 MPa, at around 600°–700°C before it decreases rapidly, due to the transformation from body-centered cubic ferrite to close-packed face-centered cubic austenite and stress temperature dependence, to below about 50 MPa at a temperature of around 900°C. On further heating, the compressive stress increases slightly, due to thermal expansion of the austenite, until the yield stress is reached and the σ-T curve starts to follow the austenite yield stress curve. During cooling, the sample starts to contract and the stress changes from compression to tension. The tensile stress reaches the yield stress for austenite and follows this stress until decomposition of austenite starts. In some cases, the stress relief due to volumetric expansion during phase transformation and associated transformation plasticity results in compressive stresses in the sample. Ferrite has high yield strength at low temperatures and thus there is lower compensation of contraction by plastic relaxation. As a result, the stress rises sharply after transformation is exhausted. The rapid buildup of tensile stress gives rise to residual stresses above 430 MPa for all specimens.

The current experiments show that the sample with a peak temperature of 1350°C and fastest cooling rate ($\Delta t_{8/5}$ around 10 s) has lowest transformation temperature and

Table 1 — Chemical Composition and Mechanical Properties of Current X70 Steel

	Elements (wt-%)												
C	Si	Mn	P	S	Cr	Ni	Al	Cu	Mo	Nb	V	Ti	N
0.09	0.30	1.71	0.012	0.001	0.07	0.05	0.05	0.04	0.02	0.05	0.01	0.02	0.005

YS = 581 MPa, UTS = 645 MPa, El = 21%

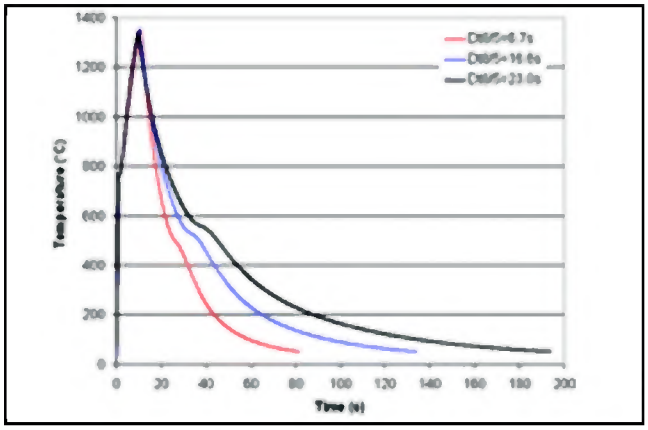

Fig. 4 — Measured temperature-time curves for samples with peak temperatures of around 1350°C.

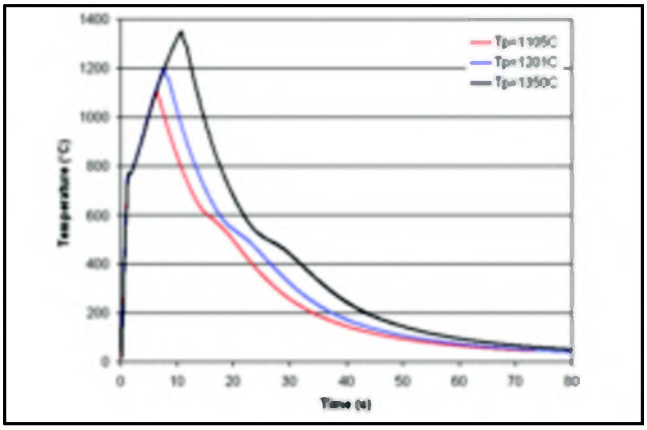

Fig. 5 — Measured temperature-time curves for samples with cooling time $\Delta t_{8/5}$ of around 10 s.

highest final stress — Fig. 5. In agreement with the CCT diagram of Fig. 1, the results show that phase transformation upon cooling occurs at lower temperatures when the $\Delta t_{8/5}$ is decreased as indicated by the stress relaxation associated with transformation plasticity. Given austenite has a higher thermal expansion coefficient than ferrite (α_γ = 2.09×10^{-5} K^{-1}, α_α = 1.29×10^{-5} K^{-1}) (Ref. 16), one would expect that transformation at lower temperatures allows larger compensation of the accumulated thermal contraction strain. As a result, lower residual stresses would be expected for samples transforming at lower temperatures compared to samples transforming at higher temperatures (Ref. 17). The CCT diagram for this material (Fig. 1) shows that this sample contains a significantly higher amount of martensite giving rise to higher low-temperature strength (Ref. 16). Thus, the yield stress is not reached before the experiment is terminated such that a high residual stress is built up. The two samples with peak temperatures of about 1350°C and $\Delta t_{8/5}$ of around 15 and 20 s have higher transformation temperatures, resulting in lower strength of the material, such that the σ-T curve follows the yield curve from about 130°C to ambient temperature — Figs. 6, 7. Similarly, samples with peak temperatures around 1200° and 1100°C and $\Delta t_{8/5}$ of around 15 and 20 s reach the yield stress before the experiment is terminated, while the sample with the fastest cooling rate ($\Delta t_{8/5}$ around 10 s), does not reach its yield limit, producing the highest final stress.

Samples with peak temperatures of around 1350°C reach higher final stress than samples with peak temperatures of 1200° and 1100°C — Fig. 8. This behavior is probably due to the increase in grain size with increasing temperature giving rise to enhanced hardenability, and thus higher strength. The grain growth is facilitated by the dissolution of precipitates at temperatures above around 1100°C (Refs. 18–20) giving rise to the decrease of the austenite strength during heating of the specimens to temperatures above around 1100°C, as seen in the σ-T curves in Figs. 6 and 7.

Effect of Preloading on the Evolution of σ-T Curves

When the samples are preloaded with a high compressive stress at the start of the experiment, further increase of compressive stress due to thermal expansion occurs at a much slower rate compared to the

Table 2 — Experimental Program

Thermal Influence	Initial Stress State	1st Cycle T_p(°C)	1st Cycle $\Delta t_{8/5}$(s)	2nd Cycle T_p(°C)	2nd Cycle $\Delta t_{8/5}$ (s)	3rd Cycle T_p(°C)	3rd Cycle $\Delta t_{8/5}$ (s)
Single cycle	Neutral	1100	10	—	—	—	—
		1100	15	—	—	—	—
		1100	20	—	—	—	—
		1200	10	—	—	—	—
		1200	15	—	—	—	—
		1200	20	—	—	—	—
		1350	10	—	—	—	—
		1350	15	—	—	—	—
		1350	20	—	—	—	—
	Compression	1200	10	—	—	—	—
		1200	15	—	—	—	—
	Tension	1200	10	—	—	—	—
		1200	15	—	—	—	—
Double cycle	Neutral	1200	15	800	15	—	—
		1200	15	1000	15	—	—
		1200	15	1100	15	—	—
		1200	15	1200	15	—	—
Triple cycle	Neutral	1200	15	1200	15	800	15

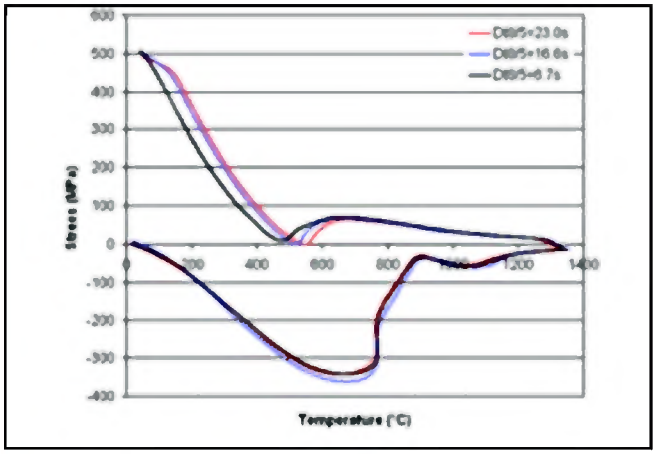

Fig. 6 — Effect of cooling rate on σ-T curves obtained for samples with peak temperatures of around 1350°C.

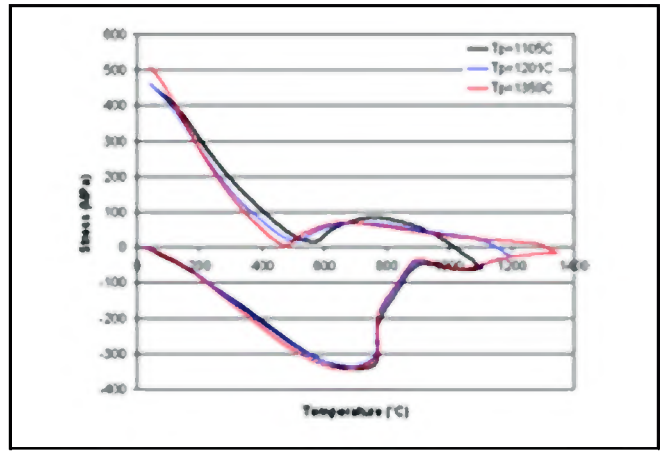

Fig. 7 — Effect of peak temperature on σ-T curves obtained for samples with cooling time $\Delta t_{8/5}$ of around 10 s.

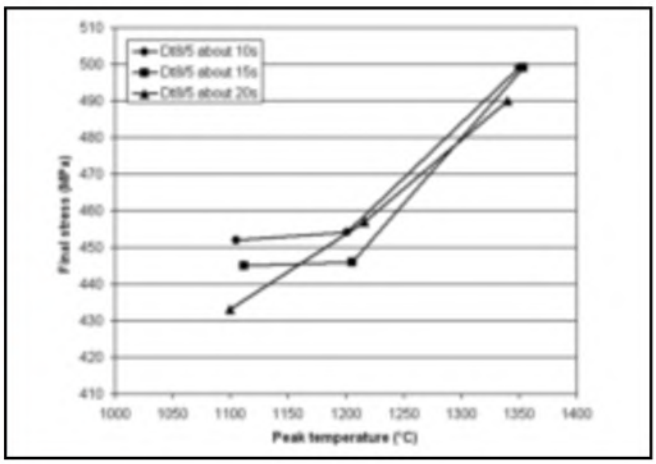

Fig. 8 — Effect of peak temperature on final stress in Satoh experiments.

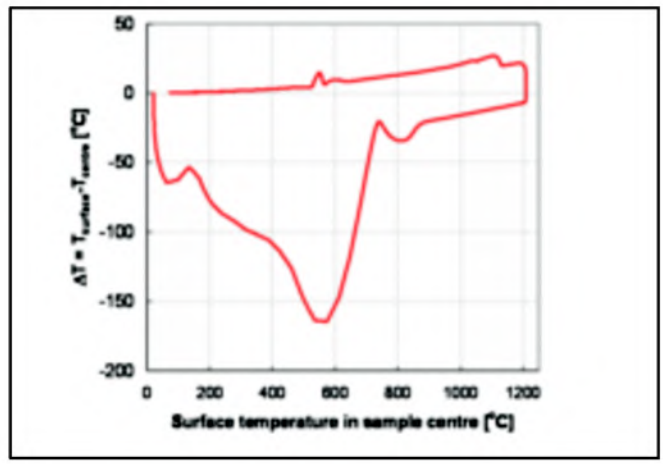

Fig. 9 — Modeled temperature difference between surface and center of the Satoh test sample. Conditions correspond to the case of a peak temperature of 1200°C.

experiments with no preloading. The maximum compressive stress for the sample with a compressive preload of 462 MPa was found to be 570 MPa at a temperature of 460°C. The very high compressive stress observed is just below the room temperature yield stress of the material, and thus well above the expected yield strength at this temperature (Ref. 21). The reason for this behavior must be a fairly steep temperature gradient within the sample such that the surface of the sample, where the temperature is measured, reaches high temperature faster than the interior of the sample. This is verified by mathematical modeling of the temperature distribution, using the FEM code *WeldsimS* (Ref. 14). In the modeling, a quarter of the sample geometry of Fig. 2 has been employed due to symmetry reasons and the measured temperature history at the surface has been imposed as a thermal boundary condition. (Refer to Ref. 16 for more details about the simulation conditions.) Figure 9 shows the calculated temperature difference between the surface and center of the samples as a function of temperature. A further increase in the temperature results in a rapid reduction of the compressive stress reflecting the yield curve of the material at increasing temperature. The samples with a high tensile preload expand such that the tensile stress is reduced as the temperature is raised. At a temperature of about 660°C, the stress changes from tensile to compressive. At a temperature just above the onset of the ferrite-to-austenite transformation, the σ-T curve for the preloaded samples reaches the σ-T curve for the sample with no preload and follows this curve very closely throughout the experiment — Fig. 10. The effect of preloading on the shape of the σ-T curve is negligible for temperatures above the A_{c1} temperature, i.e., the phase transformation relaxes the effect of different initial stresses, and the final stress level is very similar in the three different cases.

Multiple Cycle Experiments

The measured temperature cycle for the sample with first peak temperature of 1210°C and second peak temperature of 771°C is shown in Fig. 11. Similar temperature-time curves were also measured for the experiments characterized by a first peak temperature of about 1200°C and second peak temperatures of 1024°, 1114°, and 1221°C, and cooling times $\Delta t_{8/5}$ of about 15 s, respectively. The σ-T curves for the first cycle evolves in the same manner as the σ-T curves for the single-cycle experiments. When the cooling is interrupted by a new heating cycle, the second σ-T cycle starts at a high tensile stress level, typically 400–425 MPa at 150°C, which is approximately the same tensile stress level as the single-cycle experiments starting in tension — Fig. 10. Upon further heating, the σ-T curve of the second cycle meets the σ-T curve of the first cycle around the A_{c1} temperature and both curves follow the same path until the peak temperature of the second cycle is reached. During cooling, the σ-T curve of the second cycle reaches the yield stress for austenite and follows this curve until transformation of austenite commences, i.e., a similar be-

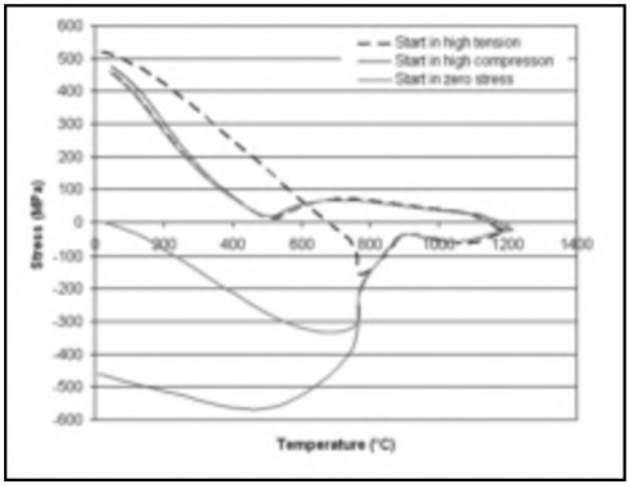

Fig. 10 — Effect of preloading on appearance of σ-T curve.

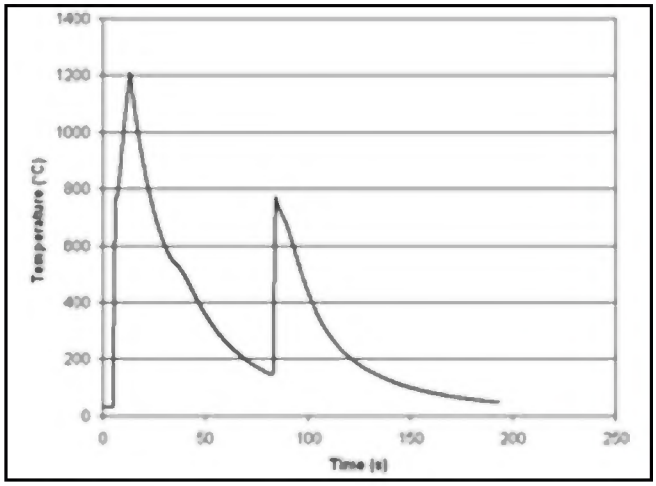

Fig. 11 — Typical measured temperature-time curve for double thermal cycle experiment.

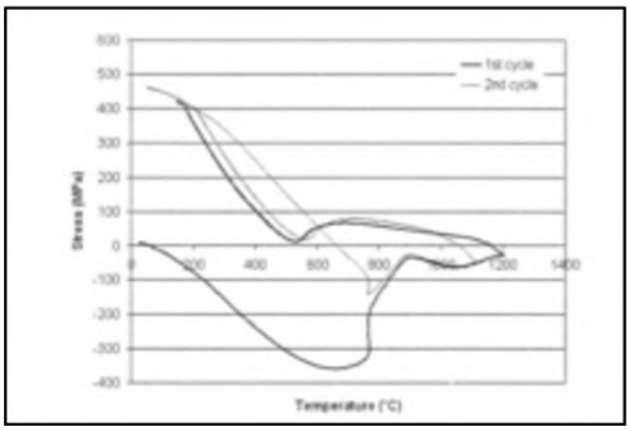

Fig. 12 — σ-T curve obtained for double thermal cycle experiment with first peak temperature of about 1200°C and second peak temperature of about 1000°C.

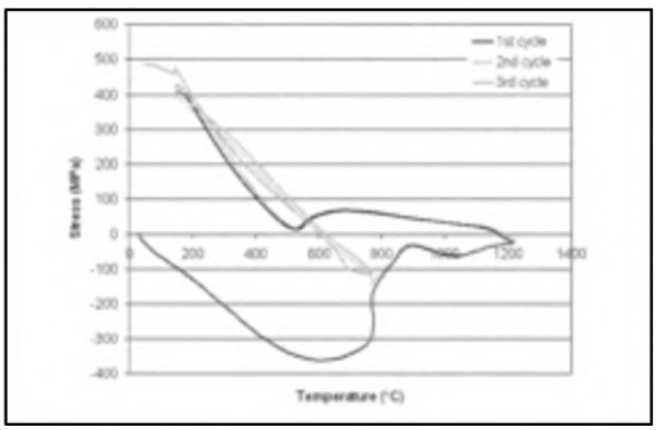

Fig. 13 — σ-T curve obtained for triple thermal cycle experiment with first and second peak temperature of about 1200°C and third peak temperature of about 800°C.

havior as obtained after the first cycle. Compared to the first cycle, the austenite-to-ferrite transformation occurs at lower temperatures as the second-cycle peak temperature increases, reflecting the increase in hardenability as a result of increased grain growth at higher peak temperatures. After completion of the transformation, the tensile stress increases rapidly to a residual stress level of 450–480 MPa when the experiment is finished. An example of a σ-T curve for a double-cycle experiment is shown in Fig. 12.

One experiment was performed using triple thermal cycles, the σ-T curve for this experiment is shown in Fig. 13. Here, the first and the second temperature cycle had peak temperature of around 1200°C and the measured σ-T curve for the two first cycles is very similar to the σ-T curve for the double-cycle experiment using peak temperatures of 1200°C. The third cycle, having a peak temperature of 769°C behaves very similarly to the last cycle of the double-cycle experiment with a peak temperature of 771°C. Thus, the effect of multiple cycles on the shape of the σ-T curve and on the final stress level is low, probably because of relaxation of strains during the phase transformations.

Relation with Base Metal Strength Level

The general rule of thumb is that the welding residual stresses are of the same order of magnitude as the base metal yield strength. This may be true as long as the solid-state phase transformations do not influence the development of residual stresses. Practical experience based on the Satoh testing has demonstrated that the extent of phase transformation influence depends on the steel transformation behavior, i.e., its hardenability. In the present case, phase transformations cause substantial changes in the residual stress buildup. The presently examined X70 pipeline steel has a yield strength of 581 MPa (Table 1). Residual stresses in the range from 433 to 499 MPa, corresponding to 75–86% of the base metal yield strength, were measured. Similar previous examinations (Ref. 22) have revealed that the residual stress of conventional C-Mn steel with base metal yield strength of 398 MPa was found to be 465 MPa at its maximum in Satoh testing, which is 117% of its yield strength. For QT steel with a yield strength of 780 MPa, the maximum residual stress was 582 MPa, which is only 75% of the $R_{p0.2}$ value (Ref. 23). The most remarkable deviation from the yield strength level has recently been reported from Satoh testing (Ref. 24) and real weld measurements (Refs. 25, 26) for supermartensitic stainless steel, where the martensite transformation takes place at very low temperatures, typically within the range of 180°–220°C. This prevents extensive buildup of residual stresses after completion of the phase transformation resulting in residual stresses being as low as about 100 MPa.

Comparison with Measurements Made on Real Welds

Although the Satoh test does not replace real weldments, it provides a quick

and inexpensive way to evaluate the residual stress potential in the HAZ by weld simulation. In a real weld, the buildup of residual stresses is obviously much more complex since the joint configuration and geometry will influence the restraint intensity, and hence the residual stresses. Moreover, in a real weld the residual stress distribution is important. In a pipeline, welding residual stresses in different directions will develop, e.g., hoop stresses and axial stresses. With either bending or tension forces acting on the pipeline, it is most relevant to compare residual stress levels in the Satoh test with the maximum axial stresses resulting from girth welding. Data from girth welding of X70 pipeline have recently been published using neutron diffraction measurements (Ref. 27). Here, axial tensile stresses in the range of 269–486 MPa were measured. Actually, the present final stresses measured in the Satoh test fall within the scatter band for the axial stresses in the real girth weld. The weld simulation experiments gave a scatter from 433 to 499 MPa, depending on the peak temperatures and cooling rates employed. Good correlation between maximum residual stresses found in the Satoh test and maximum values measured in real welds have previously been reported for C-Mn and QT steels (Ref. 15).

Summary and Conclusions

The forces caused by the constrained expansion and contraction of X70 pipeline steel specimens, subjected to simulated weld thermal cycles, have been measured by means of Satoh testing. Based on the conducted work, the following main conclusions can be drawn:

- Phase transformations cause substantial changes in the residual stress buildup for the studied X70 pipeline steel. Residual stress of 433 to 490 MPa has been recorded using the Satoh testing method. These stresses are 75–86% of the base metal yield strength.
- X70 steel samples with low austenite transformation temperature may build up higher residual stress than samples with higher austenite transformation temperature, if the transformation product in the first case has higher yield strength and the transformation product in the second case reaches its yield limit.
- Samples with peak temperatures of around 1350°C reach higher final stress than samples with peak temperatures of 1200° and 1100°C. This is probably caused by increased hardenability as a result of enhanced grain growth at higher temperatures.
- In Satoh-type experiments, the effect of preloading on the shape of the σ-T curve disappears at temperatures above the A_{c1} temperature, i.e., the phase transformation relaxes the different initial stresses and the final stress level is very similar for samples starting in high compression, high tension or zero stress.
- The effect multiple cycles on the shape of the σ-T curve and on the final stress level is low, probably because of relaxation of strains during the phase transformations.

Acknowledgment

The authors gratefully acknowledge the financial support from the Norwegian Research Council through the Resia STORFORSK project (No. 167397/V30).

References

1. Bhadeshia, H. K. D. H. in *Handbook of Residual Stresses and Deformation of Steel.* 2002. G. Totten, M. Howes, and T. Inoue, eds. Materials Park, Ohio: ASM International. pp. 1–10.

2. Withers, P. J., and Bhadeshia, H. K. D. H. 2001. Residual stress Part 1 — Measurement techniques. *Materials Science and Technology* (17): 355–365.

3 . Withers, P. J., and Bhadeshia, H. K. D. H. 2001. Residual stress Part 2 — Nature and origins. *Materials Science and Technology* (17): 366–375.

4 . Bonner, N. 1996. Measurement of residual stresses in thick section steel welds. PhD dissertation, University of Bristol, UK.

5. Arai, Y., Kikuchi, M., Watanabe, T., and Nagaki, M. 1995. Residual stresses due to welding and its effect on the assessment of cracks near the weld interface. *International Journal of Pressure Vessels and Piping* (63): 237–248.

6. Lorentzen, T., and Leffers, T. 1992. Measurement of residual and applied stress using neutron diffraction. (216) NATO ASI Series E (ed. M. T. Hutchings and A. D. Krawitz), Dordrecht, Kluwer: 253–261.

7. Gao, H., Guo, H., Blackburn, J. M., and Hedricks, R. W. 1998. Determination of residual stresses by X-ray diffraction in HSLA-100 steel weldments. *Proc. 5th Int. Conf. on Residual Stresses*, June 16–18, 1997, Linköping, Sweden, pp. 320–325.

8. Holden, T. M., Root, J. H., Fidleria, V., Holt, R. A., and Roy, G. 1988. Application of neutron diffraction to engineering problems. *Materials Science Forum* (27/28): 359–370.

9. Park, M. J., Yang, H. N., Jang, D. Y., Kim, J. S., and Jin, T. E. 2004. Residual stress measurement on welded specimen by neutron diffraction. *Journal of Materials Processing Technology* (155-156): 1171–1177.

10. Chang, K-H., and Lee, C-H. 2007. Residual stresses and fracture mechanics analysis of a crack in welds of high strength steels. *Engineering Fracture Mechanics* (74): 980–994.

11. Toyoda, M., and Mochizuki, M. 2004. Control of mechanical properties in structural steel welds by numerical simulation of coupling among temperature, microstructure, and macro mechanics. *Science and Technology of Advanced Materials* (5): 255–266.

12. Satoh, K. 1972. Thermal stresses developed in high-strength steels subjected to thermal cycles simulating weld heat affected zone. *Transactions of the Japan Welding Society* 3(1): 135–142.

13. Satoh, K. 1972. Transient thermal stresses of weld heat affected zone by both-ends-fixed analogy. *Transactions of the Japan Welding Society* 3(1): 125–134.

14. Fjær, H. G., Liu, J., Mhamdi, M., and Lindholm, D. 2006. On the use of residual stresses from welding simulations in failure assessment analyses for steel structures. *Proc. 8th Int. Seminar on Numerical Analyses of Weldability*, September 25–27, 2006, Seggau Graz, Austria.

15. Volden, L. 1999. Residual stresses in weldments. PhD dissertation, NTNU, Trondheim, Norway.

16. Onsøien, M. I., M'hamdi, M., and Mo, A. 2009. A CCT diagram for an offshore pipeline steel of X70 type. *Welding Journal* 88(1): 1-s to 6-s.

17. Bhadeshia, H. K. D. H. 2004. Developments in matrensitic and bainitic steels: role of the shape deformation. *Materials Science and Engineering A* (378): 34–39.

18. Alberry, P. J., Chew, B., and Jones, W. C. K. 1977. Prior austenite grain growth in heat affected zone of a 0.5Cr-Mo-V steel. *Metal Technology* (4): 317–325.

19. Andersen, I., and Grong, Ø. 1995. Analytical modelling of grain growth in metals and alloys in the presence of growing and dissolving precipitates-I. Normal grain growth. *Acta Metallurgica et Materialia* 43(7): 2673–2688.

20. Hashimoto, T., Komizo, Y., Sawamura, T., Nakade, H., and Nakatsuka, Y. 1986. High strength hot-bent pipe for arctic use. *Transactions of the Iron and Steel Institute of Japan* 26(5): 418–424.

21. Bredenbruch, K., Gehrmann, R., Schmidt, T., and Träger, C. 2006. Strength derating of pipeline steels at elevated temperature. *3R International* 1: 38–41.

22. Gundersen, Ø., Volden, L., Zhang, Z., Rørvik, G., and Akselsen, O. M. 1999. Modelling residual stresses in weld simulated restrained C-Mn steel specimen. *Proc. 9th ISOPE Int. Conf. (ISOPE'99)*, Brest, France, May 30–June 4, Vol. IV: 187–194.

23. Volden, L., Gundersen, Ø., and Rørvik, G. 1999. Development of residual stresses in high strength low alloy steel. *Proc. 9th ISOPE Int. Conf. (ISOPE'99)*, Brest, France, May 30–June 4, Vol. IV: 134–139.

24. Akselsen, O. M., Aune, R., Olden, V., and Rørvik, G. 2007. Effects of phase transformations on residual stresses in welding of stainless steels. *International Journal of Offshore and Polar Engineering* 17: 145–151.

25. Aune, R., Fostervoll, H., and Akselsen, O. M. 2003. Hydrogen assisted cracking in welding of 13% Cr supermartensitic stainless steels. *Proc. 22nd Int. Conf. Offshore Mechanics and Arctic Engineering (OMAE 2003)*, Cancun, Mexico, paper No. 37282.

26. Griffiths, A., Nimmo, W., Roebuck, B., Hinds, G., and Turnbull, A. 2004. A novel approach to characterising the mechanical properties of supermartensitic 13Cr stainless steel welds. *Materials Science and Engineering A* (384): 83–91.

27. Law, M., Prask, H., Luzin, V., and Gnaeupel-Herold, T. 2006. Residual stress measurements in coil, linepipe and girth welded pipe. *Materials Science and Engineering A* (437): 60–63.